

## DIRECT NUMERICAL SIMULATIONS OF THE $\kappa$ -MECHANISM

Gastine, T.<sup>1</sup> and Dintrans, B.<sup>1</sup>

**Abstract.** We present a purely-radiative hydrodynamic model of the  $\kappa$ -mechanism that sustains radial oscillations in Cepheid variables. We determine the physical conditions favourable for the  $\kappa$ -mechanism to occur by the means of a configurable hollow in the radiative conductivity profile. By starting from these most favourable conditions, we complete nonlinear direct numerical simulations (DNS) and compare them with the results given by a linear-stability analysis of radial modes. We find that well-defined instability strips are generated by changing the location and shape of the conductivity hollow. For a given position in the layer, the hollow amplitude and width stand out as the key parameters governing the appearance of unstable modes driven by the  $\kappa$ -mechanism. The DNS confirm both the growth rates and structures of the linearly-unstable modes. The nonlinear saturation that arises is produced by intricate couplings between the excited fundamental mode and higher damped overtones. These couplings are measured by projecting the DNS fields onto an acoustic subspace built from regular and adjoint eigenvectors and a 2:1 resonance is found to be responsible for the saturation of the  $\kappa$ -mechanism instability.

### 1 Introduction

Eddington (1917) discovered an excitation mechanism of stellar oscillations that is related to the opacity in ionisation regions: the  $\kappa$ -mechanism. This mechanism can only occur in regions of a star where the opacity varies so as to block the radiative flux during compression phases (Zhevakin 1953; Cox 1958). Ionisation regions correspond to a strong increase in opacity, leading to the “opacity bumps” that are responsible for the local driving of modes. These ionisation regions have nevertheless to be located in a very precise region of a star, neither too close to the surface nor too deep into the stellar core, in order to balance the damping that occurs in other regions. It defines the so-called *transition region* which is the limit between the quasi-adiabatic interior and the strongly non-adiabatic surface. For classical Cepheids that pulsate on the fundamental acoustic mode, this transition region is located at a temperature  $T \simeq 40\,000$  K corresponding to the second helium ionisation (Baker & Kippenhahn 1965). However, the bump location is not solely responsible for the acoustic instability. A careful treatment of the  $\kappa$ -mechanism would involve dynamical couplings with convection, metallicity effects and realistic equations of state and opacity tables (Bono et al. 1999). The purpose of our model is to simplify the hydrodynamic approach while retaining the *leading order* phenomenon -the opacity bump location- such that feasible DNS of the  $\kappa$ -mechanism can be achieved.

### 2 Hydrodynamic model

We focus our study on radial modes propagating in Cepheids and thus only consider the 1-D case. Our model represents a *local zoom* about an ionisation region and is composed by a monatomic and perfect gas ( $\gamma = c_p/c_v = 5/3$ ), with both a constant gravity  $\vec{g}$  and a constant kinematic viscosity  $\nu$ . The ionisation region is represented by a parametric conductivity hollow that mimics a bump in opacity as (Gastine & Dintrans 2008a):

$$K_0(T) = K_{\max} \left[ 1 + \mathcal{A} \frac{-\pi/2 + \arctan(\sigma T^+ T^-)}{\pi/2 + \arctan(\sigma e^2)} \right] \quad \text{with } \mathcal{A} = \frac{K_{\max} - K_{\min}}{K_{\max}} \quad \text{and } T^\pm = T - T_{\text{bump}} \pm e, \quad (2.1)$$

where  $T_{\text{bump}}$  is the hollow position in temperature, while  $\sigma$ ,  $e$  and  $\mathcal{A}$  denote its slope, width and relative amplitude, respectively. Examples of common values of these parameters are provided in Fig. 1.

<sup>1</sup> Laboratoire d’Astrophysique de Toulouse-Tarbes, CNRS et Université de Toulouse, 14 avenue Edouard Belin, F-31400 Toulouse, France

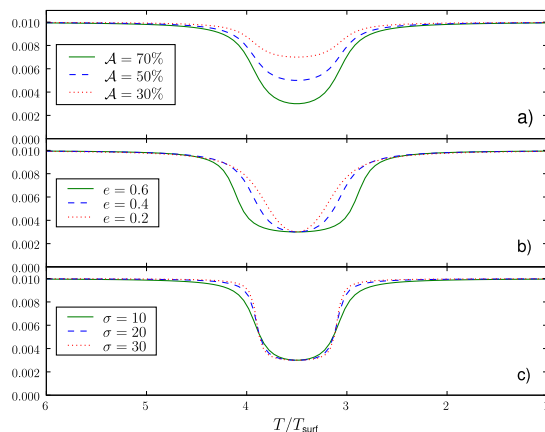


**Fig. 1.** Influence of the hollow parameters on the conductivity profile for  $K_{\max} = 10^{-2}$  and  $T_{\text{bump}} = 3.5$ : amplitude  $\mathcal{A}$  (a), width  $e$  (b) and slope  $\sigma$  (c).

### 3 Linear stability analysis

We are interested in small perturbations about the hydrostatic and radiative equilibria. The layer is fully radiative and the radiative flux perturbation reads under the diffusion approximation:

$$\vec{F}' = -K_0 \vec{\nabla} T' - K' \vec{\nabla} T_0, \quad (3.1)$$

where the “0” subscripts mean equilibrium quantities and primes denote Eulerian ones. The linearised perturbations obey to the following dimensionless equations:

$$\left\{ \begin{array}{l} \lambda T' = \frac{\gamma}{\rho_0} \left( K_0 \frac{d^2 T'}{dz^2} + 2 \frac{dK_0}{dz} \frac{dT'}{dz} + \frac{d^2 K_0}{dz^2} T' \right) - (\gamma - 1) T_0 \frac{du}{dz} + \frac{F_{\text{bot}}}{K_0} u, \\ \lambda u = -\frac{\gamma - 1}{\gamma} \left( \frac{dT'}{dz} + \frac{d \ln \rho_0}{dz} T' + T_0 \frac{dR}{dz} \right) + \frac{4}{3} \nu \left( \frac{d^2 u}{dz^2} + \frac{d \ln \rho_0}{dz} \frac{du}{dz} \right), \\ \lambda R = -\frac{du}{dz} - \frac{d \ln \rho_0}{dz} u, \end{array} \right. \quad (3.2)$$

where  $R \equiv \rho'/\rho_0$  denotes the density perturbation,  $u$  the velocity,  $F_{\text{bot}}$  the imposed bottom flux. We seek normal modes of the form  $\exp(\lambda t)$  with  $\lambda = \tau + i\omega$  (unstable modes correspond to  $\tau > 0$ ).

In order to investigate the influence of the hollow shape on stability, we fix the value of  $\sigma$  and vary the other parameters ( $T_{\text{bump}}$ ,  $\mathcal{A}$  and  $e$ ). For each case, we first compute the equilibrium fields and second, the eigenvalues with their corresponding eigenvectors are completed using the LSB spectral solver (Valdettaro et al. 2007). Figure 2 displays the obtained instability strips for the fundamental mode and two main results appear: (i) a particular region in the layer ( $T_{\text{bump}} \in [1.8, 2.3]$ ) favours the appearance of unstable modes; (ii) both a minimum width and amplitude ( $e_{\min} \simeq 0.15$  and  $\mathcal{A}_{\min} \simeq 45\%$ ) are needed to destabilise the system.

### 4 Direct numerical simulations

To confirm the instability strips discovered previously in the linear-stability analysis, we perform direct numerical simulations of the *nonlinear* problem. We start from the favourable initial conditions determined by the previous parametric surveys and advance in time the hydrodynamic equations thanks to the high-order finite-difference Pencil Code<sup>2</sup>.

<sup>2</sup>See <http://www.nordita.org/software/pencil-code> and Brandenburg & Dobler (2002).

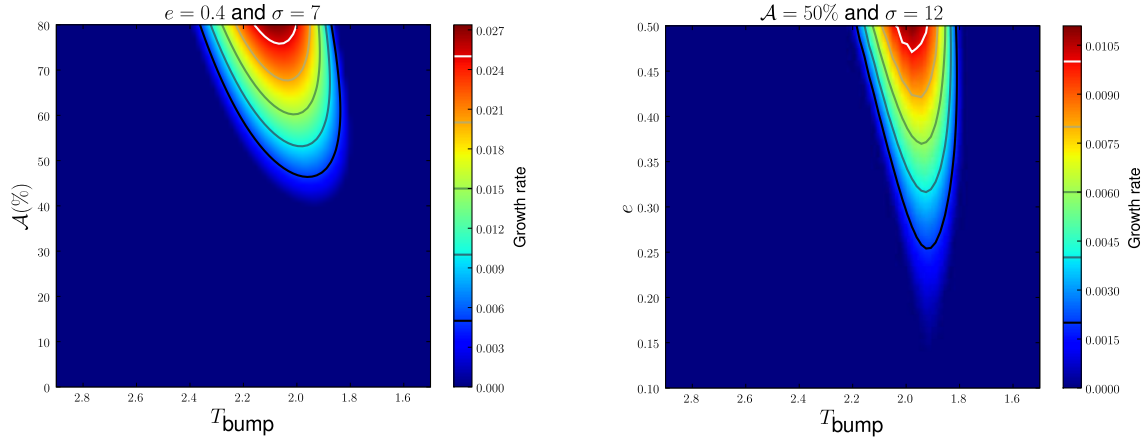


**Fig. 2.** *Left panel:* Instability strip for the fundamental mode in the plane  $(T_{\text{bump}}, \mathcal{A})$  for  $e = 0.4$ ,  $\sigma = 7$ . *Right panel:* Instability strip for the fundamental mode in the plane  $(T_{\text{bump}}, e)$  for  $\mathcal{A} = 50\%$ ,  $\sigma = 12$ .

To determine which modes are present in the DNS in the nonlinear-saturation regime, we first perform a temporal Fourier transform of the momentum field  $\rho u(z, t)$  and plot the resulting power spectrum in the  $(z, \omega)$ -plane (Fig. 3a, left). With this method, acoustic modes are extracted because they emerge as “shark fin profiles” about definite eigenfrequencies (Dintrans & Brandenburg 2004). We next integrate  $\widehat{\rho u}(z, \omega)$  over depth to obtain the mean spectrum (Fig. 3b, left). Several discrete peaks corresponding to normal modes appear but the fundamental mode close to  $\omega_0 = 5.439$  clearly dominates. Finally, the linear eigenfunctions are compared to the mean profiles computed from a zoom taken in the DNS power spectrum about eigenfrequencies  $\omega_0 = 5.439$  and  $\omega_2 = 11.06$  (Fig. 3c, left). The agreement between the linear-stability analysis (eigenfunctions in dotted blue lines) and the DNS (profiles in solid black lines) is remarkable. In summary, Fig. 3 (left) shows that several overtones are present in this DNS, even for long times. However, because these overtones are linearly stable, some underlying energy transfers must occur between modes through nonlinear couplings.

To study this nonlinear interaction, we adopt a powerful method already used to study the sound generation by airplanes in aeroacoustics or by compressible convection in astrophysics (Bogdan et al. 1993). It is based on the projection of the DNS fields onto a basis shaped from the regular and adjoint eigenvectors that are solutions to the linear-oscillation equations. By using projections onto these two respective sets of eigenvectors, the time evolution of each acoustic mode propagating in the DNS is obtained. The kinetic energy content of each mode is also available in this formalism, highlighting the energy transfer between modes. As our problem only consists in an initially static radiative zone, the velocity field that develops is only due to acoustic modes, that is,

$$E_{\text{kin}}^{\text{tot}} = E_{\text{waves}} = \sum_{n=0}^{\infty} E_n, \quad (4.1)$$

where  $E_n$ , is the energy contained in the  $n$ -acoustic mode.

The right panel of Fig. 3 displays the time evolution of the kinetic energy content  $E_n/E_{\text{kin}}^{\text{tot}}$  for  $n \in \llbracket 0, 6 \rrbracket$ . After the linear transient growth of the fundamental mode, a given fraction of energy is progressively transferred to upper overtones and the nonlinear saturation is achieved above  $t \simeq 150$ . These nonlinear couplings mainly involve the  $n = 0$  and  $n = 2$  modes because their energy ratios are dominant (more than 98% of the total energy). The reason for this favored coupling lies in the period ratio existing between these two modes: the fundamental period is  $P_0 = 2\pi/\omega_0 \simeq 1.155$ , while the  $n = 2$  one is  $P_2 \simeq 0.568$  such that the corresponding period ratio is close to one half ( $P_2/P_0 \simeq 0.491$ ). This  $n = 2$  mode, which represents about 10% of the total kinetic energy, is involved in the nonlinear saturation of the  $\kappa$ -mechanism instability through a 2:1 resonance with the fundamental mode. Such a resonance is usual in celestial mechanics with, e.g., Jupiter’s moons Io ( $P = 1.769\text{d}$ ), Europa ( $P = 3.551\text{d}$ ) and Ganymede ( $P = 7.154\text{d}$ ) and it is well known that it helps to stabilise orbits. In our case, this stabilisation takes the form of a nonlinear saturation: the linear growth of the fundamental mode is balanced by the pumping of energy from the linearly-stable second overtone behaving in that case as an energy sink, leading to the full limit-cycle stability.

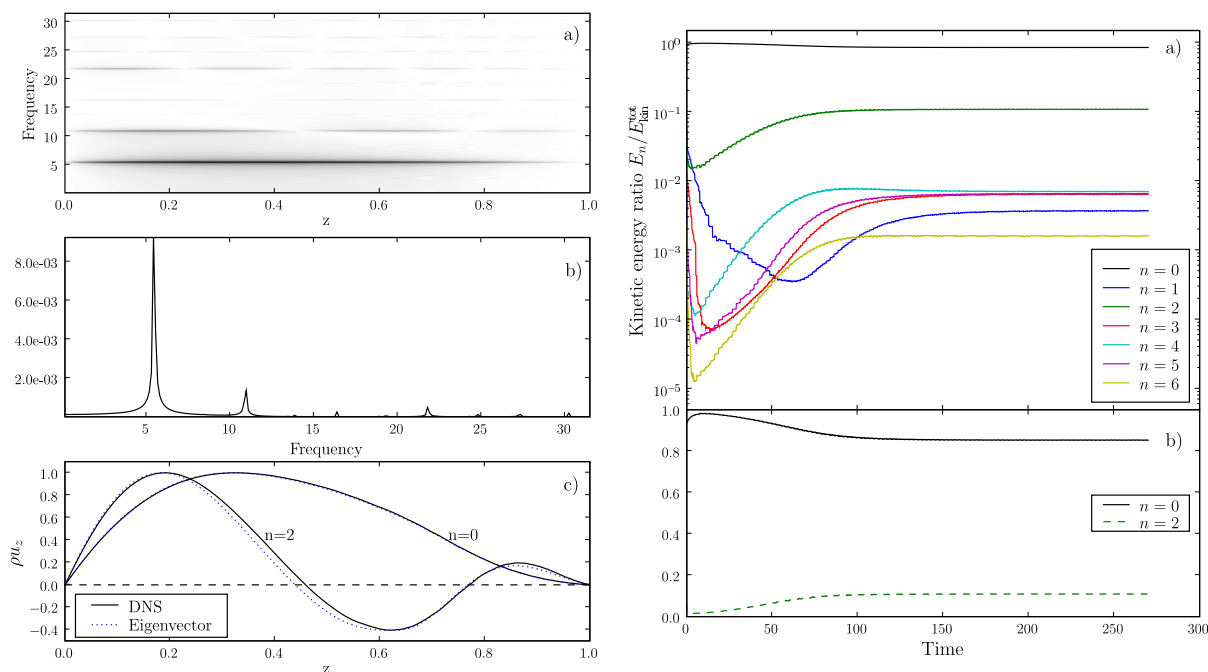


**Fig. 3.** *Left panel:* **a)** Temporal power spectrum for the momentum in the  $(z, \omega)$  plane. **b)** The resulting mean spectrum after integrating in depth. **c)** Comparison between normalised momentum profiles for  $n = (0, 2)$  modes according to the DNS power spectrum (solid black lines) and the linear-stability analysis (dotted blue lines). *Right panel:* **a)** Kinetic energy ratio for  $n \in [0, 6]$  in a logarithmic  $y$ -scale. **b)** Zoom for the  $n = 0$  and  $n = 2$  modes only.

## 5 Conclusion

Direct numerical simulations (DNS) of the  $\kappa$ -mechanism that excite stellar oscillations are performed. We first compute the most favourable setups using a linear-stability analysis of radial modes propagating in a 1-D layer of gas. In our model, a configurable hollow in the radiative conductivity profile mimics the opacity bump responsible for the layer destabilisation. The instability strips found in the linear study are outstandingly confirmed by the DNS and we show that the nonlinear saturation that arises involves a 2:1 resonance between the linearly-unstable fundamental mode and the linearly-stable second overtone.

## References

- Baker, N. & Kippenhahn, R. 1962, *Zeitschrift für Astrophysik*, 54, 114
- Bogdan, T. J., Cattaneo, F., & Malagoli, A. 1993, *ApJ*, 407, 316
- Bono, G., Marconi, M., & Stellingwerf, R. F. 1999, *ApJS*, 122, 167
- Brandenburg, A. & Dobler, W. 2002, *CoPhC*, 147, 471 [[arXiv:astro-ph/0111569](#)]
- Cox, J. P. 1958, *ApJ*, 127, 194
- Dintrans, B. & Brandenburg, A. 2004, *A&A*, 421, 775 [[arXiv:astro-ph/0311094](#)]
- Eddington, A. S. 1917, *The Observatory*, 40, 290
- Gastine, T. & Dintrans, B. 2008, *A&A*, 484, 29 [[arXiv:astro-ph/0711.1276](#)]
- Gastine, T. & Dintrans, B. 2008, *A&A*, in press [[arXiv:astro-ph/0804.0345](#)]
- Valdettaro, L., Rieutord, M., Braconnier, T. & Fraysse, V. 2007, *JCoAM*, 205, 382 [[arXiv:physics/0604219](#)]
- Zhevakin, S. A. 1953, *Russ. A. J.*, 30, 161